A Method for Optimizing the Artifact Subspace Reconstruction Performance in Low-Density EEG

Andrea Cataldo, *Senior Member, IEEE*, Sabatina Criscuolo, Egidio De Benedetto, *Senior Member, IEEE*, Antonio Masciullo, Marisa Pesola, Raissa Schiavoni, and Sara Invitto

***Abstract*— Electroencephalogram (EEG) plays a significant role in the analysis of cerebral activity, although the recorded electrical brain signals are always contaminated with artifacts. This represents the major issue limiting the use of EEG in daily life applications, as artifact removal process still remains a challenging task. Among the available methodologies, Artifact Subspace Reconstruction (ASR) is a promising tool that can effectively remove transient or large-amplitude artifacts. However, the effectiveness of ASR and the optimal choice of its parameters have been validated only for high-density EEG acquisitions. In this regard, the present study proposes an enhanced procedure for the optimal individuation of ASR parameters, in order to successfully remove artifact in low-density EEG acquisitions (down to four channels). The proposed method starts from the analysis of real EEG data, to generate a large semi-simulated dataset with similar characteristics. Through a fine-tuning procedure on this semi-simulated data, the proposed method identifies the optimal parameters to be used for artifact removal on real data. The results show that the algorithm achieves an efficient removal of artifacts preserving brain signal information, also in low-density EEG signals, thus favoring the adoption of EEG also for more portable and/or daily-life applications.**

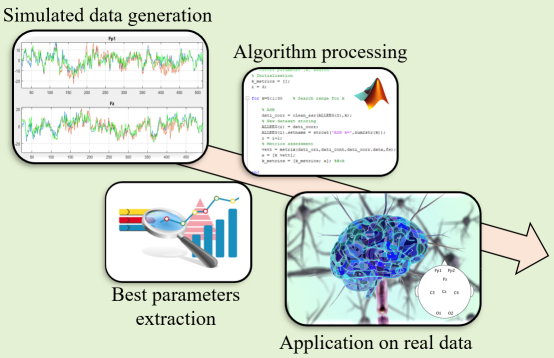

***Index Terms*— electroencephalography, EEG, low density system, artifact removal, Artifact Subspace Reconstruction, ASR, BCI, measurement system**

I. Introduction

ELECTROENCEPHALOGRAPHY (EEG) is a well-established neuroimaging technique largely used to analyze brain activity, mostly in clinics and laboratories [1], [2]. Indeed, new EEG-based applications for more practical use are being investigated, thanks to its non-invasiveness, ease of use, and potential wearability and portability [3]–[7]. However, the use of EEG outside of clinical and research settings is still limited because the cerebral signal is heavily influenced by noise and interference, leading to a variety of artifacts [8] that compromise the correct extraction of the features of interest [9]. Artifacts can be caused either by non-physiological [10] or physiological sources [11]. The latter, which are more difficult to remove [12], are due for example to eye movements, blinks, and muscle activity [13]–[15]. As a result, EEG data is a non-stationary, non-linear stochastic mixture of brain signals and artifacts. The removal of EEG artifacts and the identification of interfering signals outcomes are a critical pre-processing step for the correct measurement of neuro-physiological phenomena of interest related to brain activity [16], [17]. At the state of the art, there are many techniques and algorithms developed for *artifact removal*, which can be grouped into four major categories: *regression methods*, *filtering methods*, *blind source separation methods* (BSS), and *source decomposition methods* [11], [18]–[21]. However, such techniques often require the use of additional reference channels (e.g., electrooculography, electromyography) or classifiers to identify and discard artifact-related components. Additionally, they carry a high

Submitted in August 2022.
This work was supported in part by the INTENSE project (F/310148/01-05/X56)— Italian Ministry of Economic Development Accordo Innovazione DM 31/12/2021.

A. Cataldo, A. Masciullo, and R. Schiavoni are with the University of Salento - Department of Engineering for Innovation, 73100 Lecce, Italy (e-mail: andrea.cataldo@unisalento.it)

S. Criscuolo, and E. De Benedetto are with the University of Naples Federico II - Department of Electrical Engineering and Information Technology (DIETI), 80125 Naples, Italy (e-mail: egidio.debenedetto@unina.it)

M. Pesola is with the University of Naples Federico II - Center for Advanced Metrological and Technological Services (CeSMA), 80146 Naples, Italy

S. Invitto is with the University of Salento - Dept. of Biological and Environmental Sciences and Technologies, 73100 Lecce, Italy.

The EEG data used for the generation of the simulated data were acquired by the DREAM Neuroscience Laboratory in Vito Fazzi Hospital in Lecce, Italy. Data collection was performed in accordance with the Helsinki Declaration, and written informed consent was obtained from all participants. This study was carried out in accordance with the recommendations of Ethical Committee of Vito Fazzi Hospital, Lecce (Italy).

computational burden [22]. Indeed, there is still no agreement on an optimal removal technique for all types of artifacts. Several factors, such as the total number of channels, the need for a reference channel, and the characteristics of the chosen algorithm (e.g., linearity, automation, and online applicability), need to be considered in practice. These factors may lead to increased system noise and complexity, but also to an increased user discomfort. The total number of channels, in particular, limits the ability to successfully remove artifacts; only a few algorithms are suitable for single-channel and multichannel applications [23].

To overcome these limitations, the *Artifact Subspace Reconstruction* (ASR) method has been proposed in recent years as an online, automatic, component-based artifact removal method for nonstationary large-amplitude or transient artifacts [24], [25]. As observed in the literature, the ASR method holds unexplored potential, although recent studies have reported promising results [26]–[28]. These works have mainly focused on using ASR to remove artifacts from high-density EEG acquisitions, typically using suboptimal default ASR parameters. However, it has recently been demonstrated that ASR performs better than other multi-channel techniques as the number of channels decreases by down to four [29]. Moreover, excellent performance of ASR has been demonstrated in removing artifacts on 8-channel Steady-State Visual Evoked Potentials signals [30]. Nevertheless, its application and optimization for low-density EEGs is still in question.

Based on these considerations, this study proposes a method for tuning ASR parameters in order to make artifact removal more efficient by considering 8, 6 and 4 channels. In doing so, not only the user-defined *ASR Rejection Threshold Parameter k* but also the *ASR sliding window length wl* were investigated. However, tuning these two parameters directly on real data is not possible, since the original pure signal is not available to calculate comparison metrics and quantify the efficiency of the correction. Thus, the basic idea of the proposed method lies in the generation of semi-simulated data with characteristics similar to the real available data to be processed. Once the algorithm is tuned on the semi-simulated data, it is possible to find the best ASR parameters values to apply on the real data.

The outline of this paper is as follows. Section II provides the background on the ASR algorithm. Section III outlines the proposed method and the metrics used to evaluate its performance. Section IV describes the data used in this study and the implementation of the proposed approach. Finally, Section V reports the results obtained applying the proposed approach on semi-simulated data and real data.

II. Background

The basic concept of the ASR process is the extraction of reference statistics from an artifact-free data segment to calibrate the correction of contaminated data [24]. High-amplitude non-stationary artifacts, such as muscle artifacts and eye blinks, are identified and rejected with an automatic thresholding in the domain of the principal components (PCs).

The ASR process consists of three major steps [22]:

1) *Extraction of reference data*. A portion of the signal without artifacts is identified by calculating the root-mean-square (RMS) values on 1-second sliding windows for each channel. Then, z-score is computed along the entire channel to assess the dispersion degree and discern clean reference data. A minimum 30-second/1-minute length is usually recommended for reference data, but the duration can vary.

2) *Threshold definition to identify artifact components*. After an Infinite Impulse Response (IIR) filtering, a mixing matrix is calculated as the square root of the covariance matrix of the filtered reference data. Furthermore, the eigenvectors are used to project onto the PC space. In the projected space, RMS values with mean μ_i and standard deviation σ_i are calculated on sliding windows of the new data. The default *sliding window length (wl)* is set at $0.5\,\mathrm{s}$. Then, a rejection criterion Γ_i is determined by a user-defined *cutoff threshold parameter* (k) multiplied by the standard deviation:

$$\Gamma_i = \mu_i + k \cdot \sigma_i. \tag{1}$$

The cutoff parameter k establishes how aggressively faulty data are removed. Smaller values of k are associated with higher aggressiveness.

3) *Artifact component rejection and signal reconstruction*. Finally, the transformation procedures of the second step are applied to the uncleaned EEG data. For each window, the algorithm identifies which principal component exceed the rejection threshold Γ_i in the projection space. Artifact components that fulfill the criterion are set to zero before reconstructing the cleaned signal.

Hence, the ASR algorithm performance is heavily influenced by user-selected parameters, in particular the already mentioned *cutoff threshold parameter (k)* and *sliding window length (wl)*. However, as reported in Section I, the majority of ASR-based works use standard parameters [24], [30]. Studies focusing on the optimal value of k, in particular, revealed that this value could be between 20 and 30, which is small enough to remove artifact and preserve most of brain information [27], [22].

III. Proposed Method

The proposed method allows for the customization of ASR parameters to improve artifact removal. Starting from semi-simulated data, the two considered parameters k and wl are optimized, and then their best values are applied to the real data. Figure 1 describes this three-step procedure in full depth.

1) Preliminary analysis of real EEG data and generation of semi-simulated dataset: At this phase, the real EEG data corrupted by artifacts are preliminary analysed. The data are analyzed both in the time and frequency domain in order to identify some characteristics, such as artifact type and duration, amplitude and sampling rate. In particular, semi-simulated EEG data are generated with the same channels and sampling rate as the real data. A further check was

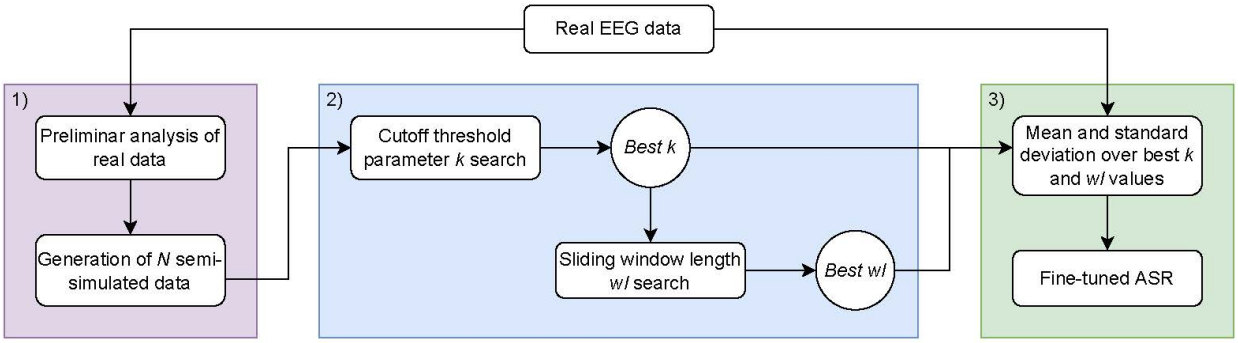

Fig. 1: Pipeline of the proposed method for fine-tuning ASR parameters

then made in terms of comparing the amplitudes of the two EEGs through the evaluation of the mean and the standard deviation of the signal in time domain and, finally, the spectral similarity of the semi-simulated and real EEG signals was quantified by comparing the two Power Spectral Density (PSD). Based on these considerations, semi-simulated data are generated to reflect the available real data characteristics.

2) ASR parameters customization: This step provides a first search to investigate aggressive and non-aggressive values of k at a fixed value of wl. Then, once the best value for k was calculated, the wl value was parameterized.
Regarding the automatic choice of the best k and wl values, it was carried out considering three metrics between pure and corrected signals: Root Mean Square Error (RMSE), Gamma Value (γ) and Correlation Coefficient (ρ). Each of these metrics measures quantitatively how well the EEG dataset has been corrected and it can be calculated for the entire EEG trace and for specific signal conditions, i.e. with muscular or ocular artifacts. Then, an auto-select function determines the k and wl that optimize the greatest number of metrics on the different segments of the signals. In addition to this quantitative evaluation, the results were visually inspected.
The procedure was iterated by determining the best k and wl parameters on the the whole semi-simulated data set.

3) Application of k and wl values to real data: The mean and standard deviation of the best k and wl values obtained in the preceding step are computed. On real data, extreme and average values of the obtained range are used in the ASR algorithm. The effectiveness of artifact removal is evaluated through visual inspection.

A. Metrics for Automatic Choice of k and wl

On semi-simulated data, several metrics can be found in literature to evaluate the artifact removal performance. Some of them rely on the evaluation of the distortion in each specific band of EEG signal [31]. However, this kind of approach is not adequate for efficient numerical computation and does not preserve the overall power of the EEG signal. Starting from these considerations, in this work, the following three metrics were chosen [32]:

1) RMSE: This is an absolute error measure in which deviations are squared to prevent positive and negative values from cancelling each other out. With this measure, larger value errors are also amplified, a feature that can facilitate the elimination of methods with the most significant errors. The RMSE formula is:

$$\sqrt{\sum_{i=1}^{n} \frac{(EEG_{corr,i} - EEG_{true,i})^2}{N}} \tag{2}$$

where EEG_{true} is the original simulated EEG dataset, EEG_{corr} is the corrected dataset after ASR and N is the number of samples of data. In an ideal case of the corrected signal being perfectly equal to the true signal, the RMSE would be equal to 0.

2) Gamma Value γ: An efficient parameter for evaluating artifact removal enhancements is artifact removal gain γ. It is defined as the ratio between two different signal-to-artifact ratio (SAR):

$$\gamma = 10 \cdot log\left(\frac{SAR_A}{SAR_B}\right) \tag{3}$$

where SAR_B is the signal-to-artifact ratio between EEG_{true} and contaminated EEG signal (EEG_{cont}), while SAR_A is the signal-to-artifact ratio between EEG_{true} and EEG_{corr}. Therefore, γ value also takes into account the contribution of the corrupted EEG signal, which is not the case of RMSE, and this makes the parameter particularly useful. It is clear that positive gamma values identify an improved signal-to-noise ratio, while negative values indicate a decrease, and zero is no improvement at all.

3) Cross-correlation: Cross-correlation is a measure of similarity of two signals as a function of a time shift or translation applied to one of them. For EEG_{true} and EEG_{corr} discrete functions, the cross-correlation is defined as:

$$(EEG_{true} * EEG_{corr})[n] = \sum_{m=-\infty}^{\infty} EEG_{true}[m] EEG_{corr}[m+n] \tag{4}$$

where n is called displacement or lag and the complex conjugate of the signal does not appear since the EEG is a

real signal. Since there is no interest in the translation of the signals, we considered the cross-correlation value for n=0, normalized between -1 and 1.

The automatic choice of k and wl parameters is made by selecting the parameters in order that:

- the Root Mean Square Error between EEG_{true} and EEG_{corr} was minimum,
- the Gamma Value and Correlation Coefficient between EEG_{true} and EEG_{corr} was maximum.

IV. Implementation

In this section, the implementation of the proposed method is described in detail.

A. Description of the Data Sets

1) Real Data: Real EEG data were collected from a publicly available dataset in order to test artifact removal techniques [33]. Each trace was recorded with a Brain Products helmet with 27 EEG channels and 3 electrooculographic channels [34] at a sampling rate of 1000 Hz and then made available at a resampling rate of 200 Hz. This dataset contains clean and contaminated data from one recording session for each of the 13 subjects. Data were collected over the course of two experimental sessions. The first phase required participants to focus their attention on a fixation cross on a screen while avoiding movement. In this way, 30 seconds of clean signal (baseline) was acquired for each subject. Participants in the second phase performed muscular and ocular artifacts guided by cues on the screen. In a random order, ten repetitions of nine different types of artifacts were performed, for a total length of 40 min to 50 min. To reduce computational costs, the entire EEG trace was trimmed. The two baseline segments, in particular, were preserved, as were nine subsequent contaminated segments from the artifact conditions. Furthermore, eight channels were extracted to assume a few-channel acquisition. In the end, the raw EEG traces were base-normalized and filtered. As well known, base-normalization allows for a signal normally distributed, whereas filtering is a preprocessing step fundamental to improve the signal-to-noise ratio, by attenuating noisy frequencies. As a matter of fact, EEG signals can often be exposed to strong power line interference at 50 or 60 Hz or can be influenced by the presence of a DC offset. For this reason, filtering is a good practice before the subsequent processing. Table I summarizes real data characteristics.

TABLE I: Summarized characteristics of real data and semi-simulated

	Real data	**Semi-simulated data**
Baseline	60 s	60 s
Artifacts	60 s	60 s
Sampling frequency	1000 Hz	256 Hz
Re-sampling frequency	200 Hz	200 Hz

2) Semi-simulated Data: Pure EEG signals were simulated with the generation function of the *MRC EEG data simulator* available online [35]. To simulate pure signal, a duration of 120 s and a sampling frequency of 256 Hz were chosen. The first 60 s of the trace were fully preserved to represent clean calibration data (baseline) for ASR applications, while the remaining 60 s were contaminated with real ocular and muscle artifacts. The used real artifact segments were extracted from the online *DenoiseNet database* [36] and combined with the pure semi-simulated data. In order to obtain 30 s of muscular artifacts and 30 s of ocular artifacts, 15 2 s-long segments for each artifact kind were randomly extracted and combined. To properly combine these signals, the artifact amplitude was scale-adapted to obtain a signal-to-noise ratio from -20 dB to 5 dB [37]. Furthermore, the inclusion of ocular artifacts was weighed channel-wise due to different propagation of eye components over the scalp [38]. The weights for eight selected channels were determined by calculating the correlation coefficients between genuine electrooculographic data and the matching EEG real data [39]. Ocular artifacts were more visible in the frontal and occipital areas [40], whereas the central area was thought to better appreciate muscle movements [41]. Table II summarizes the selected channels and the aforementioned correlation coefficients.

The whole simulation process was repeated 20 times in order to obtain different virtual subjects with a random choice of the artifacts. Finally, all the semi-simulated signals were filtered and re-sampled to match real data characteristics, as shown in Table I. The spectral similarity of two EEG sets was quantified by comparing the PSD of each semi-simulated data to the PSD of one of the real sources.

TABLE II: Correlation coefficients to weigh ocular artifacts.

Channel	Fp1	Fp2	Fz	C3	Cz	C4	O1	O2
Weight	1	1	0.73	0.24	0.01	0.12	0.31	0.28

B. Algorithm Implementation

As described in Section III, the method proposed in this study entails first fine-tuning the parameters on a semi-simulated dataset, based on the real data, followed by applying the mean of best results obtained on synthetic data to real data.

More in detail, the generated semi-simulated signal was processed in *MATLAB* through *EEGLAB*, an open-source toolbox for EEG analysis [42]. With a focus on low-density EEG, the number of acquisition channels was reduced from eight (Table II), associated with the brain areas mainly considered in BCI applications, to six channels (excluding $Fp1$ and $C4$) and then to four channels (excluding Cz and $O1$). The channels were reduced randomly, with at least one related to the brain areas initially considered remaining.

The ASR algorithm was implemented with *clean_rawdata()* EEGLAB plug-in, by using the *clean_asr.m* function. The basic principle is to find a baseline and perform statistics on it. With a sliding window on the data, the function searches the sub-spaces where activity deviates from the baseline. Then, the bad sub-spaces are treated as missing data and their contents

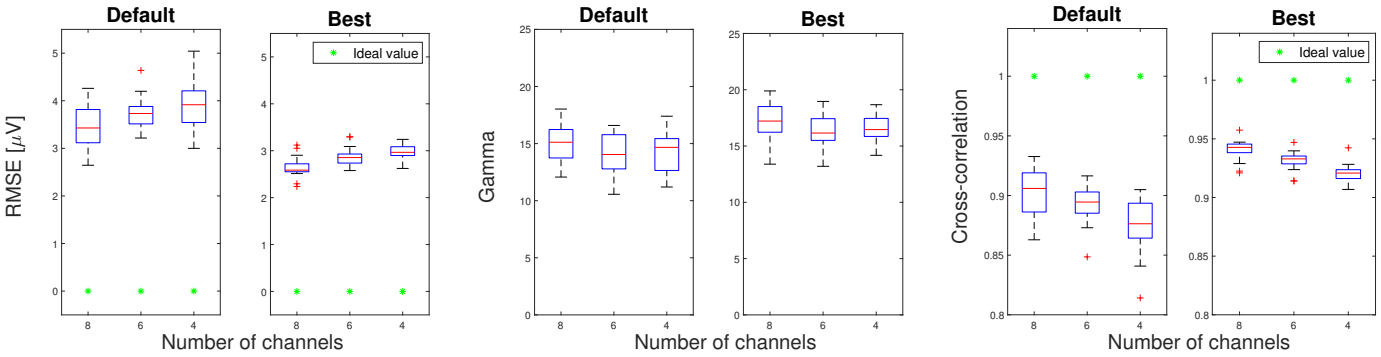

Fig. 2: Boxplot for all the semi-simulated data when the number of channels decreases. The three considered metrics are calculated on the entire EEG trace. Red line: median value; blue box: interquartile range; red cross: outlier.

are reconstructed by using statistics calculated on clean data, ensuring the data does not contain unusually strong power.
As mentioned in Section III, the present study focused on adjusting k and wl user-selected parameters to improve artifact removal with the ASR algorithm. In particular:

- *k search* has been made by varying k in a range from 5 to 30 with 1 step. Quite conservative value is 20, which is default *clean_asr.m* function parameter.
- *wl [s] search*, once the best value for k, has been performed by changing its value in a range from $0.2\,\mathrm{s}$ to $2\,\mathrm{s}$, with $0.1\ \mathrm{s}$ step. The default *clean_asr.m* function value is $0.5\ \mathrm{s}$.

Before applying ASR, real raw signals were base-normalized and filtered with the EEGLAB functions *pop_rmbase.m* and *pop_eegfiltnew.m*. In particular, the EEG signals were filtered with a high-pass filter to filter out slow frequencies less than 0.5 Hz and with a notch filter (48-52 Hz) to eliminate the line interference at 50 Hz.

The described algorithm to optimize ASR parameters was made available at `https://github.com/anthonyesp/low_density_eeg_asr.git`.

V. Experimental Results

The procedure described in the previous sections was first tested on 20 randomly generated semi-simulated EEG traces and, subsequently, was applied on the real EEG data. More in detail, the results obtained on the semi-simulated data allow to highlight the effectiveness of the automatic optimization algorithm in choosing the best ASR parameters. Finally, the best k and wl parameters in terms of the mean of all values obtained from the 20 iterations of the procedure, were used on the real dataset, showing a significant improvement in ASR correction over that made with the default parameters. The procedure shows the same encouraging results at both 8- and 6- and 4-channels.

A. Results on Semi-simulated Data

As mentioned in Section III, for each configuration of the 20 semi-simulated dataset, the optimal pair of parameters in terms of k and wl was found through the use of the automatic choice procedure described in the second step of proposed method III-.2 (see Figure 1). The use of such a function based on different types of metrics allows to identify the k and wl that ensure the best correction. As a matter of fact, to assess artifact removal on each semi-simulated EEG trace, RMSE (Eq. 2), Gamma Value (Eq. 3) and Correlation Coefficient (Eq. 4) were chosen (see Section III-A). These metrics highlights the difference between the contaminated signal EEG_{cont} and the corrected signal EEG_{corr} after artifact removal.

TABLE III: Metrics values for default parameter and best parameters of a single subject

	Muscolar artifacts							
	Default parameters				Best parameters			
# Ch	RMSE	Gamma	Corr	MAE (PSD)	RMSE	Gamma	Corr	MAE (PSD)
8	4.01	22.49	0.83	14.92	3.09	24.77	0.89	11.88
6	4.61	21.27	0.79	16.47	3.45	23.70	0.87	11.76
4	4.20	22.1	0.80	13.89	3.59	23.44	0.85	11.28
	Ocular artifacts							
	Default parameters				Best parameters			
# Ch	RMSE	Gamma	Corr	MAE (PSD)	RMSE	Gamma	Corr	MAE (PSD)
8	3.55	16.54	0.86	8.37	2.93	18.2	0.89	7.66
6	3.99	14.79	0.84	10.93	3.15	16.87	0.88	8.39
4	4.04	16.21	0.81	9.86	3.58	17.26	0.83	8.98
	Total EEG trace							
	Default parameters				Best parameters			
# Ch	RMSE	Gamma	Corr	MAE (PSD)	RMSE	Gamma	Corr	MAE (PSD)
8	2.68	20.76	0.92	7.68	2.13	22.76	0.95	6.51
6	3.05	19.52	0.90	8.99	2.36	21.75	0.94	6.82
4	2.91	20.18	0.90	7.98	2.54	21.38	0.92	6.98

Table III shows the metrics values both in the case of corrected dataset with the default parameters ($k = 20$ and $wl = 0.5\,\mathrm{s}$) and in the case of the best k and wl chosen by the automatic function. To be brief, the table only includes one of the semi-simulated EEG traces. A clear improvement in terms of metrics can be noted, since the RMSE decreases ever more to 0, the correlation coefficient increases reaching nearly 1, and also the γ value increases. The efficiency of correction with the best parameters is also demonstrated by calculating mean absolute error (MAE) in power spectral density (PSD), which is a useful metric for analyzing information loss after signal correction [43]. More in detail, this metric measures the average magnitude of the errors in original signal PSD and corrected signal PSD. Therefore, in the current work, MAE-

This article has been accepted for publication in IEEE Sensors Journal. This is the author's version which has not been fully edited and
content may change prior to final publication. Citation information: DOI 10.1109/JSEN.2022.3208768

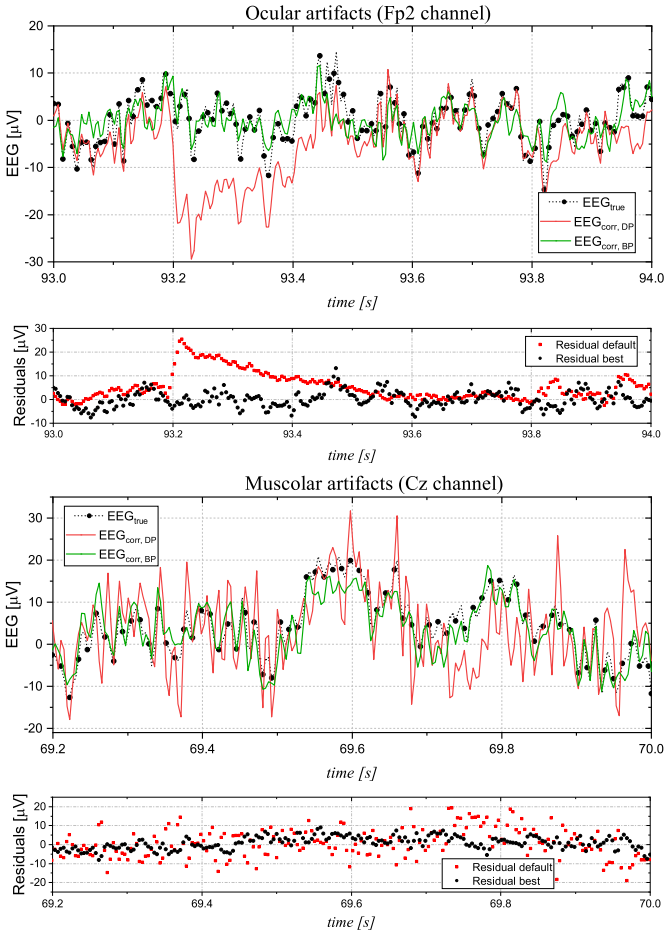

Fig. 3: Comparison between EEG_{true} (black), EEG_{corr} with default parameters (red) and EEG_{corr} with best parameters (green) traces at 8 channels. Residual panels (the difference between EEG_{true} and EEG_{corr}) for each figure are reported.

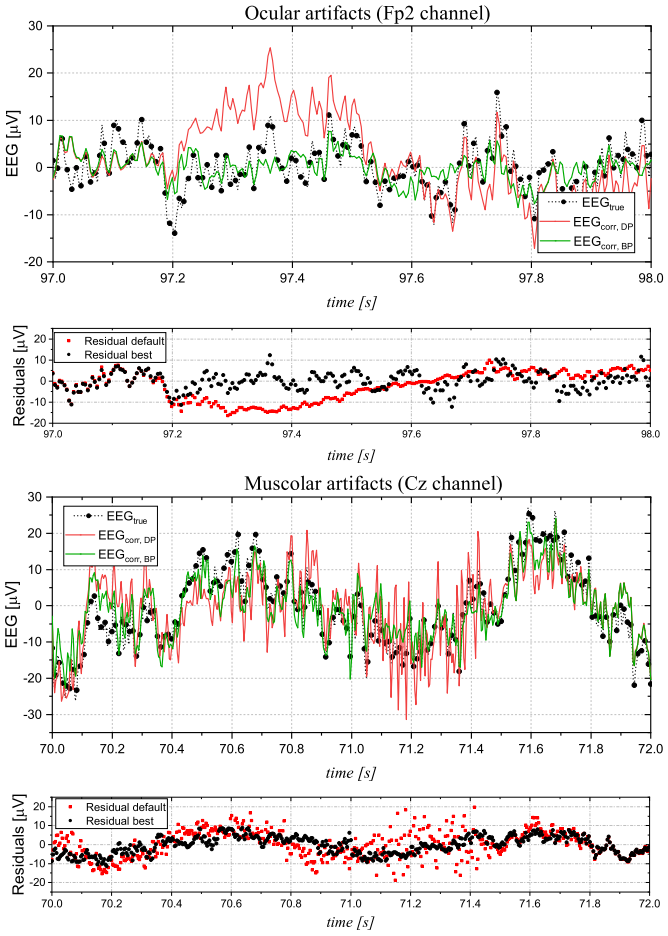

Fig. 4: Comparison between EEG_{true} (black), EEG_{corr} with default parameters (red) and EEG_{corr} with best parameters (green) traces at 6 channels. Residual panels (the difference between EEG_{true} and EEG_{corr}) for each figure are reported.

PSD values between the EEG_{true} and the EEG_{corr} with the two parameters sets, default and best, were calculated. As shown in Table III, MAE-PSD values are lower for the correct signal with the best parameters.

Instead, for an overview, the boxplots of the three metrics on the total of the semi-simulated traces are shown as the number of channels decreases in Figure 2. As can be seen, when the signal is corrected with the default parameters, the RMSE reaches a higher median value and a larger standard deviation. On the contrary, when the signal is corrected with the best parameters, the RMSE has lower median values and smaller standard deviation, approaching the ideal value of zero. Similar considerations can be made for gamma and cross-correlation. Considering both metrics, higher median values and better standard deviation ranges are observed in the case of the signal corrected with the best parameters.

The results obtained in terms of metrics and automatic choice of the best k and wl are reflected directly in the EEG trace by comparing EEG_{true} with both the dataset corrected with the default parameters $EEG_{corr,DP}$ and the dataset corrected with the best parameters $EEG_{corr,BP}$. In particular, Figure 3 represents the same simulated subject of Table III at 8 channels. For the sake of clarity, out of the eight channels, only the most significant in terms of effective removal of artifacts are reported. In particular, the Fp2 channel was chosen for ocular artifacts and the Cz and C3 channel for muscle artifacts.

It is evident in Figure 3 the $EEG_{corr,DP}$ is still compromised by artifacts. In particular, there are typical peaks of ocular artifacts for the Fp2 channel and the presence of muscle artifacts characterized by a high-frequency trend for the Cz channel. On the other hand, the $EEG_{corr,BP}$ better follows the trend of the original signal preserving its shape. Finally, Figure 4 and Figure 5 show the same results for the 6- and 4-channel case, respectively. It is clear that, even if the number of channels decreases, the algorithm works well. The results highlight how the use of the optimization algorithm allows for a much more efficient correction of the EEG data: this is evident from both the analysis of the metrics and the graphs.

B. Application on Real Data

Finally, in order to improve the process of artifacts correction and removal on real data, the optimal range for the ASR

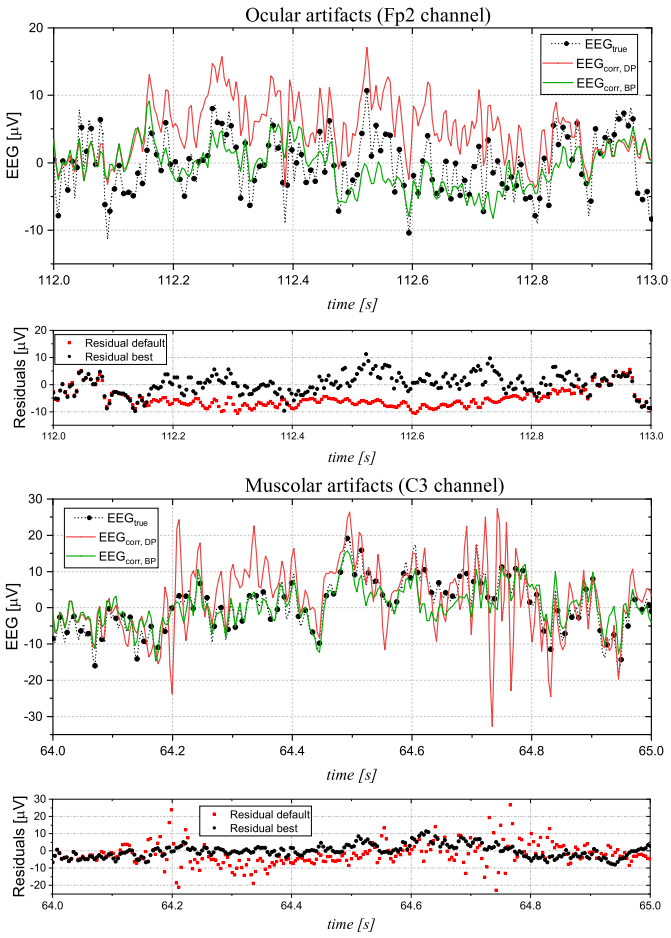

Fig. 5: Comparison between EEG_{true} (black), EEG_{corr} with default parameters (red) and EEG_{corr} with best parameters (green) traces at 4 channels. Residual panels (the difference between EEG_{true} and EEG_{corr}) for each figure are reported.

TABLE IV: Best k and wl parameters for each channel in terms of mean and standard deviation for real data

	8 channels	6 channels	4 channels
k [adim]	11.75 (4.29)	10.20 (3.59)	9.75 (2.57)
wl [s]	1.58 (0.45)	1.47 (0.55)	1.61 (0.37)

k and wl parameters was calculated based on the 20 semi-simulated dataset. As described in the third step of proposed method III-.3 (see Figure 1), the optimal range was found in terms of mean and standard deviation for each channel, as reported in Table IV. However, on real data it is not possible to use a metric that quantitatively defines the improvement in artifact correction, since in this case the EEG_{true} in unknown. Therefore, it is not possible calculate the differences between the true clean signal and the corrected signal. As a matter of fact, there is a lack of consensus between researchers on the evaluation criterion for the applied artifact removal techniques. In the recent literature, some assessment processes have been proposed but none of them still outperforms visual inspection [17]. In fact, visual inspection by an expert operator is still considered the best criterion for evaluating artifact removal techniques on real EEG data.

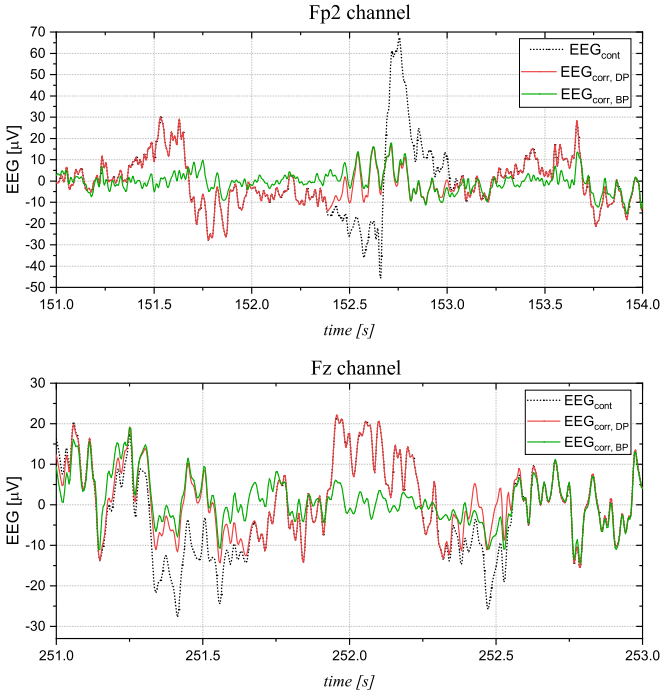

Fig. 6: Comparison between EEG_{cont} (black), EEG_{corr} with default parameters (red) and EEG_{corr} with best parameters (green) traces at 4 channels for real data EEG.

On such basis, Figure 6 shows the comparison between the original contaminated signal EEG_{cont} and the two corrected signals with the default parameters $EEG_{corr,DP}$ and with the mean of best parameters $EEG_{corr,BP}$ of Table IV. In particular, for the sake of brevity, the results obtained on only one trace of real EEG signal and only the 4-channel low-density case are shown, since it represents the most critical situation. As a matter of fact, in Figure 6 $EEG_{corr,DP}$, in some time intervals, follows the trend of the EEG_{cont}, not performing artifact removal. Indeed, the $EEG_{corr,BP}$ shows a clear removal of the remaining artifacts. This signal has amplitude values between $-10\,\mu V$ and $10\,\mu V$, an optimum range for EEG signals amplitudes. However, this is not always evident in Figure 6 for scaling reason, having to visualize on the same graph the very pronounced artifact. The clear removal of artifacts can be seen especially in the range 151-152 s and 152.5-153 s of Fp2 channel and in a small range centered on 251.5 and 252 s of Fz channel. In addition, it is worth noting how the $EEG_{corr,BP}$ follows the same trend in terms of shape as the original signal: this means that there was no over-correction or loss of information. Finally, artifact correction was also tested using the upper and lower extremes of the optimal range of Table IV for k and wl. As a matter of fact, the lower value and the upper value lead to an overcorrection and an undercorrection of some artifacts, respectively. For this reason, mean values of k and wl allow for better and more balanced results. However, in practical cases, the operator can change the parameters within the proposed range according to specific needs.

VI. Conclusions

In the present work, the performance of the ASR for the removal of artifacts in a low-density scenario was investigated. This is a promising artifact-removal technique that has been used in a variety of applications but has received little attention in the literature for low-density EEG. The goal of this research was to develop an automatic algorithm to optimize the choice of the ASR's two main user-selected parameters, namely the cutoff threshold parameter k and the sliding window length wl. Starting from semi-simulated EEG data based on the actual data at hand, the ASR was applied for a number of channels from 8 to 4. A range from 5 to 30 was explored for k, while wl was varied between $0.2\,\mathrm{s}$ to $2.0\,\mathrm{s}$. Three different metrics, RMSE, γ, and cross-correlation, were calculated on different signal segments to assess artifact removal in order to identify the best values of these parameters. For statistical significance, the algorithm was repeated on several semi-simulated traces. In each iteration, the value of k and the value of wl most voted by the considered metrics were selected. Visual inspection of signals confirmed better performance of the ASR with optimized parameter values compared to default values.

Therefore, the results of this optimization were applied on real EEG data using the average values among the best k and among the best wl. The resulting signal was then compared to the signal corrected using the default ASR configuration. Also in this case, an improvement in the removal of the ocular and muscle artifacts was observed through visual inspection. In conclusion, ASR proved to be a powerful and automatic method for removing artifacts in low-density EEG signals, which can favor the successful employment of EEG also for portable, practical applications. As a result, the proposed technique has the great advantage of identifying the fundamentals parameters of ASR to be used for a good artifact removal process on real data. In this way, artifacts can be removed more effectively than with the use of the default parameters. However, it is necessary to simulate data that is as close to the real signals as possible, in order to find the best parameters for the algorithm application on them. As mentioned above, this is related to lack of knowledge of the original pure real signal, making calculating comparison metrics between pure and corrected signals not feasible. In this regard, future work will be dedicated to overcoming this limitation by developing a quantitative metric for selecting the best parameters for removal based on real data. This, in fact, in addition to visual inspection, could enhance parameters optimization, with the purpose of embedding ASR as an online processing technique in portable systems.

Acknowledgment

The Authors would like to thank prof. Pasquale Arpaia for his insightful suggestion and theoretical support in the work.

References

[1] J. C. Henry, "Electroencephalography: basic principles, clinical applications, and related fields," *Neurology*, vol. 67, no. 11, pp. 2092–2092, 2006.

[2] P. Arpaia, A. Cataldo, S. Criscuolo, E. De Benedetto, A. Masciullo, and R. Schiavoni, "Assessment and scientific progresses in the analysis of olfactory evoked potentials," *Bioengineering*, vol. 9, no. 6, 2022.

[3] S. Saha, K. A. Mamun, K. Ahmed, R. Mostafa, G. R. Naik, S. Darvishi, A. H. Khandoker, and M. Baumert, "Progress in brain computer interface: Challenges and opportunities," *Frontiers in Systems Neuroscience*, vol. 15, p. 578875, 2021.

[4] Y. Zhang, S. Q. Xie, H. Wang, and Z. Zhang, "Data analytics in steady-state visual evoked potential-based brain–computer interface: A review," *IEEE Sensors Journal*, vol. 21, no. 2, pp. 1124–1138, 2020.

[5] T. Shi, L. Ren, and W. Cui, "Feature extraction of brain–computer interface electroencephalogram based on motor imagery," *IEEE Sensors Journal*, vol. 20, no. 20, pp. 11787–11794, 2019.

[6] P. Arpaia, E. De Benedetto, L. De Paolis, G. D'Errico, N. Donato, and L. Duraccio, "Performance enhancement of wearable instrumentation for AR-based SSVEP BCI," *Measurement*, vol. 196, 2022.

[7] A. Apicella, P. Arpaia, E. De Benedetto, N. Donato, L. Duraccio, S. Giugliano, and R. Prevete, "Enhancement of SSVEPs classification in BCI-based wearable instrumentation through machine learning techniques," *IEEE Sensors Journal*, vol. 22, no. 9, pp. 9087–9094, 2022.

[8] G. V. S. Karthik, S. Y. Fathima, M. Z. U. Rahman, S. R. Ahamed, and A. Lay-Ekuakille, "Efficient signal conditioning techniques for brain activity in remote health monitoring network," *IEEE sensors journal*, vol. 13, no. 9, pp. 3276–3283, 2013.

[9] M. Z. I. Ahmed, N. Sinha, S. Phadikar, and E. Ghaderpour, "Automated feature extraction on asmap for emotion classification using eeg," *Sensors*, vol. 22, no. 6, 2022.

[10] K. T. Sweeney, T. E. Ward, and S. F. McLoone, "Artifact removal in physiological signals—practices and possibilities," *IEEE transactions on information technology in biomedicine*, vol. 16, no. 3, pp. 488–500, 2012.

[11] J. A. Urigüen and B. Garcia-Zapirain, "Eeg artifact removal—state-of-the-art and guidelines," *Journal of neural engineering*, vol. 12, no. 3, p. 031001, 2015.

[12] W. Tatum, A. Husai, S. Benbadis, and P. Kaplan, "Normal eeg," *Handbook of EEG interpretration. USA: Demos Medical Punlishing*, pp. 1–50, 2008.

[13] R. Ranjan, B. C. Sahana, and A. K. Bhandari, "Ocular artifact elimination from electroencephalography signals: A systematic review," *Biocybernetics and Biomedical Engineering*, vol. 41, no. 3, pp. 960–996, 2021.

[14] M. Fatourechi, A. Bashashati, R. K. Ward, and G. E. Birch, "Emg and eog artifacts in brain computer interface systems: A survey," *Clinical neurophysiology*, vol. 118, no. 3, pp. 480–494, 2007.

[15] X. Chen, X. Xu, A. Liu, S. Lee, X. Chen, X. Zhang, M. J. McKeown, and Z. J. Wang, "Removal of muscle artifacts from the eeg: a review and recommendations," *IEEE Sensors Journal*, vol. 19, no. 14, pp. 5353–5368, 2019.

[16] J. Minguillon, M. A. Lopez-Gordo, and F. Pelayo, "Trends in eeg-bci for daily-life: Requirements for artifact removal," *Biomedical Signal Processing and Control*, vol. 31, pp. 407–418, 2017.

[17] W. Mumtaz, S. Rasheed, and A. Irfan, "Review of challenges associated with the eeg artifact removal methods," *Biomedical Signal Processing and Control*, vol. 68, p. 102741, 2021.

[18] X. Jiang, G.-B. Bian, and Z. Tian, "Removal of artifacts from eeg signals: a review," vol. 19, no. 5, p. 987, 2019.

[19] M. K. Islam, A. Rastegarnia, and Z. Yang, "Methods for artifact detection and removal from scalp eeg: A review," *Neurophysiologie Clinique/Clinical Neurophysiology*, vol. 46, no. 4-5, pp. 287–305, 2016.

[20] T.-P. Jung, S. Makeig, C. Humphries, T.-W. Lee, M. J. Mckeown, V. Iragui, and T. J. Sejnowski, "Removing electroencephalographic artifacts by blind source separation," *Psychophysiology*, vol. 37, no. 2, pp. 163–178, 2000.

[21] N. K. Al-Qazzaz, S. Hamid Bin Mohd Ali, S. A. Ahmad, M. S. Islam, and J. Escudero, "Selection of mother wavelet functions for multi-channel eeg signal analysis during a working memory task," *Sensors*, vol. 15, no. 11, pp. 29015–29035, 2015.

[22] C.-Y. Chang, S.-H. Hsu, L. Pion-Tonachini, and T.-P. Jung, "Evaluation of artifact subspace reconstruction for automatic artifact components removal in multi-channel eeg recordings," *IEEE transactions on biomedical engineering*, vol. 67, no. 4, pp. 1114–1121, 2020.

[23] X. Chen, A. Liu, J. Chiang, Z. J. Wang, M. J. McKeown, and R. K. Ward, "Removing muscle artifacts from eeg data: Multichannel or single-channel techniques?," *IEEE Sensors Journal*, vol. 16, no. 7, pp. 1986–1997, 2015.

[24] T. R. Mullen, C. A. Kothe, Y. M. Chi, A. Ojeda, T. Kerth, S. Makeig, T.-P. Jung, and G. Cauwenberghs, "Real-time neuroimaging and cognitive monitoring using wearable dry eeg," *IEEE Transactions on Biomedical Engineering*, vol. 62, no. 11, pp. 2553–2567, 2015.

[25] C. A. E. Kothe and T.-P. Jung, "Artifact removal techniques with signal reconstruction," Apr. 28 2016. US Patent App. 14/895,440.
[26] M. Plechawska-Wojcik, M. Kaczorowska, and D. Zapala, "The artifact subspace reconstruction (asr) for eeg signal correction. a comparative study," in *International Conference on Information Systems Architecture and Technology*, pp. 125–135, Springer, 2018.
[27] C.-Y. Chang, S.-H. Hsu, L. Pion-Tonachini, and T.-P. Jung, "Evaluation of artifact subspace reconstruction for automatic eeg artifact removal," in *2018 40th Annual International Conference of the IEEE Engineering in Medicine and Biology Society (EMBC)*, pp. 1242–1245, IEEE, 2018.
[28] B.-Y. Tsai, S. V. S. Diddi, L.-W. Ko, S.-J. Wang, C.-Y. Chang, and T.-P. Jung, "Development of an adaptive artifact subspace reconstruction based on hebbian/anti-hebbian learning networks for enhancing bci performance," *IEEE Transactions on Neural Networks and Learning Systems*, 2022.
[29] P. Arpaia, E. De Benedetto, A. Esposito, A. Natalizio, M. Parvis, and M. Pesola, "Comparing artifact removal techniques for daily-life electroencephalography with few channels," in *IEEE International Symposium on Medical Measurements and Applications*, (Taormina, Italy), 2022.
[30] V. P. Kumaravel, V. Kartsch, S. Benatti, G. Vallortigara, E. Farella, and M. Buiatti, "Efficient artifact removal from low-density wearable eeg using artifacts subspace reconstruction," in *2021 43rd Annual International Conference of the IEEE Engineering in Medicine & Biology Society (EMBC)*, pp. 333–336, IEEE, 2021.
[31] M. Saini, U. Satija, and M. D. Upadhayay, "Wavelet based waveform distortion measures for assessment of denoised eeg quality with reference to noise-free eeg signal," *IEEE Signal Processing Letters*, vol. 27, pp. 1260–1264, 2020.
[32] M. M. N. Mannan, M. A. Kamran, and M. Y. Jeong, "Identification and removal of physiological artifacts from electroencephalogram signals: A review," *Ieee Access*, vol. 6, pp. 30630–30652, 2018.
[33] S. Ehrlich, "Dataset automatic artifact removal." `https://github.com/stefan-ehrlich/dataset-automaticArtifactRemoval`.
[34] "Introducing the actichamp plus – offering active and passive electrode recordings ... and more!." `https://pressrelease.brainproducts.com/actichamp_plus/`.
[35] N. Yeung, R. Bogacz, C. B. Holroyd, and J. D. Cohen, "Detection of synchronized oscillations in the electroencephalogram: an evaluation of methods," *Psychophysiology*, vol. 41, no. 6, pp. 822–832, 2004.
[36] Ncclabsustech, "Ncclabsustech/eegdenoisenet: Eegdenoisenet, a benchmark dataset, that is suited for training and testing deep learning-based eeg denoising models, as well as for comparing the performance across different models.."
[37] M. Dora and D. Holcman, "Adaptive single-channel eeg artifact removal with applications to clinical monitoring," *IEEE Transactions on Neural Systems and Rehabilitation Engineering*, vol. 30, pp. 286–295, 2022.
[38] A. Anzolin, J. Toppi, M. Petti, F. Cincotti, and L. Astolfi, "Seed-g: simulated eeg data generator for testing connectivity algorithms," *Sensors*, vol. 21, no. 11, p. 3632, 2021.
[39] S. Invitto, A. Calcagnì, G. Piraino, V. Ciccarese, M. Balconi, M. De Tommaso, and D. M. Toraldo, "Obstructive sleep apnea syndrome and olfactory perception: An oerp study," *Respiratory Physiology & Neurobiology*, vol. 259, pp. 37–44, 2019.
[40] J. Górecka and A. Biedka, "Determination of ocular artifacts in the clinical eeg software by a peripheral device," *Electronics*, vol. 10, no. 2, p. 108, 2021.
[41] L. Frølich and I. Dowding, "Removal of muscular artifacts in eeg signals: a comparison of linear decomposition methods," *Brain informatics*, vol. 5, no. 1, pp. 13–22, 2018.
[42] A. Delorme and S. Makeig, "Eeglab: an open source toolbox for analysis of single-trial eeg dynamics including independent component analysis," *Journal of neuroscience methods*, vol. 134, no. 1, pp. 9–21, 2004.
[43] A. K. Maddirala and R. A. Shaik, "Removal of eog artifacts from single channel eeg signals using combined singular spectrum analysis and adaptive noise canceler," *IEEE Sensors Journal*, vol. 16, no. 23, pp. 8279–8287, 2016.

Andrea Cataldo (M'12, SM'13) is an Associate Professor of electric and electronic measurements with the University of Salento. He has coauthored more than 200 publications.
Prof. Cataldo is also the co-founder of the University spin-off company name Monitoring Technologies - Spin off of the University of Salento.
His research interests include reflectometry and microwave measurement techniques, uncertainty evaluation, characterization and optimization of sensors, biomedical sensors. Prof. Cataldo is a member the IEEE I&M Society and of the Italian Group of Electrical and Electronic Measurements (GMEE).

Egidio De Benedetto (M'14, SM'16) received the M.S. degree in materials engineering and the Ph.D. degree in information engineering from the University of Salento, Lecce, Italy, in 2006 and 2010, respectively.
He was with the Institute of Microelectronics and Microsystems, National Research Council, Lecce, Italy, from 2010 to 2012.
Since 2019, Egidio De Benedetto is an Associate Professor with the Department of Electrical Engineering and Information Technology of the University of Naples Federico II (Italy).

Antonio Masciullo received the M.S. degree in electronic engineering from the Polytechnic of Bari, Bari, Italy, in 1995, and the Ph.D. degree in information engineering from the University of Salento, Lecce, Italy, in 2015. He has been involved in the design and realization of electronic devices and equipment since 1997.
Since 2003, he has been with the Department of Innovation Engineering, University of Salento, where he is currently a Laboratory Technician of the Telecommunications, Automatic Control, and Electronic Measurement Laboratories.

Raissa Schiavoni received her M.S. Degree in Communication Engineering and Electronic Technologies at the University of Salento in 2020. She is currently pursuing her Ph.D. degree in Complex Systems Engineering at the University of Salento, Italy. Her research interests focus on microwave reflectometry systems for monitoring applications.

Sabatina Criscuolo received her M.S. Degree in Biomedical Engineering at the University of Naples Federico II (Naples, Italy) in 2021. She is currently pursuing her Ph.D. degree in Information and Communication Technology for Health at the University of Naples Federico II, Italy. Her research interests focus on artificial intelligence techniques and systems to support precision medicine.

Marisa Pesola received her M.S. Degree in Biomedical Engineering at the University of Naples Federico II (Naples, Italy) in 2022. Currently, she is a Research Fellow with the Center for Advanced Metrological and Technological Services (CeSMA) of the University of Naples Federico II. Her research interests focus on processing of biomedical signals and artifact removal.

Sara Invitto is an Associate Professor of General and Experimental Psychology at the University of Salento.